

Article

Exploring the Polarization of Light in Ferrofluids with Mueller Matrices

Alberto Tufaile *  and Adriana Pedrosa Biscaia Tufaile 

Soft Matter Laboratory, School of Arts, Sciences and Humanities, University of São Paulo, São Paulo 03828-000, Brazil

* Correspondence: tufaile@usp.br

Abstract: We studied the polarization of light in a thin film of ferrofluid subjected to a magnetic field using the Mueller matrix formalism. By observing the results of some experiments, we relate the observed light patterns with Stokes vectors that can be operated by Mueller matrices, which represent the magnetic field applied to the sample. We observed that the changes in the dichroism of this system can be monitored along the sample, allowing for the visualization of magneto-optical effects mainly for linear polarized light, and the effects of circular polarized light are related to birefringence.

Keywords: Mueller matrix; Stokes vector; polarization; isogyres; ferrofluid; magneto-optics



Citation: Tufaile, A.; Tufaile, A.P.B. Exploring the Polarization of Light in Ferrofluids with Mueller Matrices. *Magnetochemistry* **2022**, *8*, 121. <https://doi.org/10.3390/magnetochemistry8100121>

Academic Editor: Catalin Nicolae Marin

Received: 13 September 2022

Accepted: 4 October 2022

Published: 7 October 2022

Publisher's Note: MDPI stays neutral with regard to jurisdictional claims in published maps and institutional affiliations.



Copyright: © 2022 by the authors. Licensee MDPI, Basel, Switzerland. This article is an open access article distributed under the terms and conditions of the Creative Commons Attribution (CC BY) license (<https://creativecommons.org/licenses/by/4.0/>).

1. Introduction

Light is an electromagnetic wave, and to manipulate this type of wave we need devices with electro-optical or magneto-optical properties. In this work, we will focus on the observation of the polarization of light in a magneto-optical device known as a Ferroc cell [1], which is composed of a thin layer of ferrofluid that controls the polarization of the light incident on this layer by applying a magnetic field, based on Stokes vectors operated by matrices [2], known as Mueller matrices [3]. This type of matrix calculus is a common algebraic resource in areas that involve the study of some kind of electromagnetic scattering by particles, such as in biological applications [4–6] based on selective connective tissue staining techniques that allow a qualitative analysis of collagen fibers in connective tissue to increase birefringence in images observed in oncology tests. This includes material characterization [7,8] used to characterize chiral films that have been processed from bacterial cellulose. The matrix calculus is also used in optical device development [9], such as in polarimetric imaging analysis of optical components for the generation of cylindrical vector beams, and in astrophysics [10], where the polarization state of the radiation provides much more astrophysical information than just the light intensity; it is also used in remote sensing [11] as a tool to enhance the information available in a variety of remote sensing applications, as well as in astrobiology [12], in the study of entopic phenomenon [13], to elucidate the perception of Haidinger brushes and horocycles of light [14], which shows some of the connections between topology and optics. Mueller matrices are also used in many other areas [15].

To introduce some concepts that we will explore in this paper, we begin with the following question: what is the relationship between the polarization of light in a thin film of ferrofluid and the magnetic field applied to this sample? We can answer this question by projecting the magnetic field of a dipole \vec{p} that is distributed through space, as is shown in Figure 1a on a thin layer of ferrofluid. The expressions for the potential Φ and the magnetic field \vec{B} of a dipole \vec{p} in a point at distance \vec{r} with angle θ from the origin are given by the following equation:

$$\Phi = \frac{pz}{(x^2 + z^2)^{3/2}} \quad (1)$$

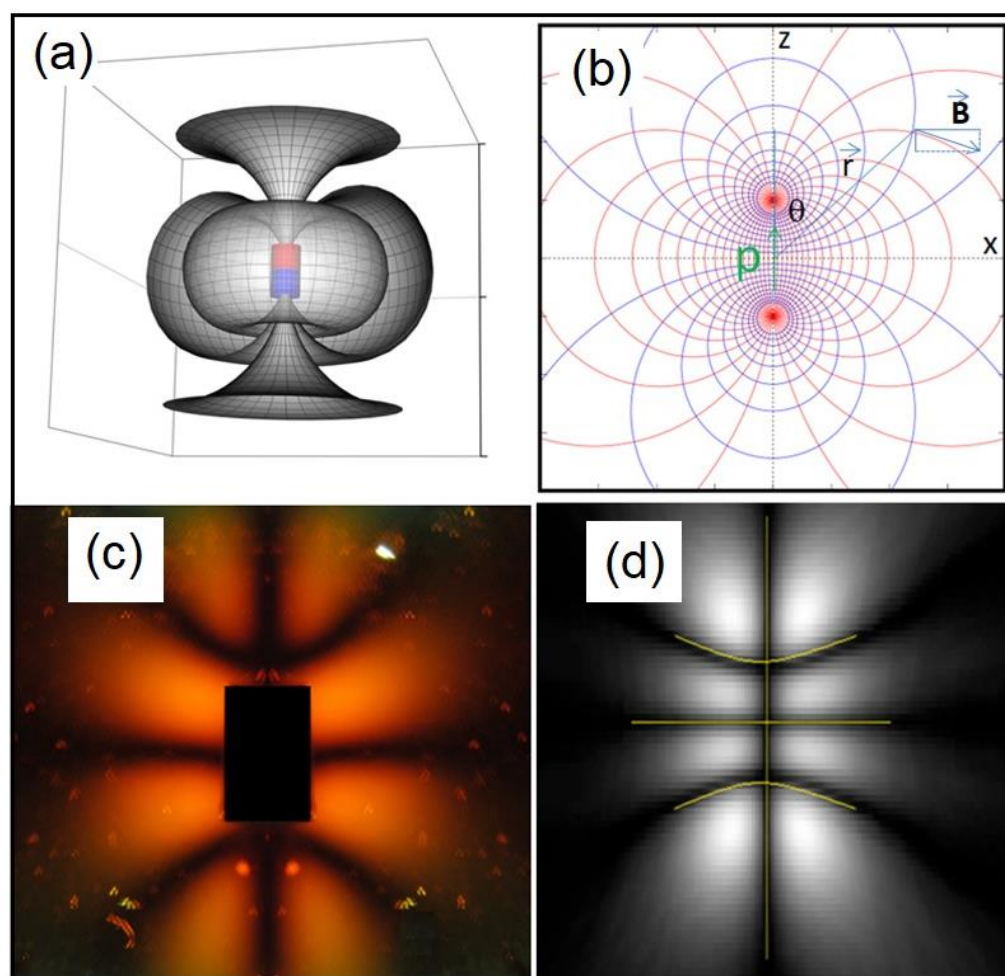


Figure 1. (a) Diagram of the magnetic field around a magnetic dipole. (b) Magnetic dipole diagram in the xz plane, with its respective dipole coordinate system. (c) Example of a luminous pattern of polarization of light in a Ferrocylinder with a magnetic dipole. (d) Diagram of a luminous pattern with isogyres marked with yellow lines.

The components of the magnetic field for the dipole are as follows:

$$B_x = \frac{3pxz}{(x^2 + z^2)^{5/2}} = \frac{3p \sin\theta \cos\theta}{r^3} \quad (2)$$

$$B_z = \left[\frac{3z^2}{(x^2 + z^2)^{5/2}} - \frac{1}{(x^2 + z^2)^{3/2}} \right] = \frac{p(3 \cos^2\theta - 1)}{r^3} \quad (3)$$

When this magnetic field with certain intensity acts on the thin film of ferrofluid, the nanoparticles align with the magnetic field, forming a diffraction grating that can polarize light. Placing this thin film of ferrofluid influenced by this magnetic field between a pair of crossed polarizers, we obtain the axially symmetrical light pattern of Figure 1c with light and dark regions. The dark regions within the pattern are a direct consequence of the alignment of the magnetic field with the orientation of one of the polarizers, since the Jones vector related to the polarization of light is perpendicular to the magnetic field; these are known as isogyres. Furthermore, in regions where the magnetic field has a weak intensity (less than 200 gauss), the grating does not form and light is not transmitted, resulting in the dark parts around the pattern. In our previous paper involving Jones vectors [9], we have

considered the electric field of the light expressed as two-component vector with $0 \leq \lambda \leq 1$; in the following, κ is an amplitude parameter [16]:

$$|E\rangle = \begin{bmatrix} E_x \\ E_y \end{bmatrix} = |E| \begin{bmatrix} \kappa \\ \sqrt{1-\kappa^2} \end{bmatrix} (e^{i\theta_M}) \quad (4)$$

In this experiment, the applied magnetic field creates a diffraction grating in the ferrofluid, rotated at angle θ_M with respect to x-axis, which is basically a projection on the operator $|T_{\theta_M}\rangle$, while the intensity I is the modulus squared of the inner product $I = |\langle T_{\theta_M}|E\rangle|^2$ of the system discussed previously, giving the following:

$$I(\theta_M) = |E|^2 [\kappa^2 \cos^2 \theta_M + (1 - \kappa^2) \sin^2 \theta_M + \kappa \sqrt{(1 - \kappa^2)} \sin 2\theta_M \cos \Delta] \quad (5)$$

where Δ is a constant related to the partial polarization of the electromagnetic wave.

To discuss the effects of the magnetic field on the polarization of light, we produced the diagram in Figure 2, where we highlight the isogyre pattern of this system with the yellow lines. The straight horizontal and vertical lines show the magnetic field on the z-axis and x-axis aligned with one of the polarizers.

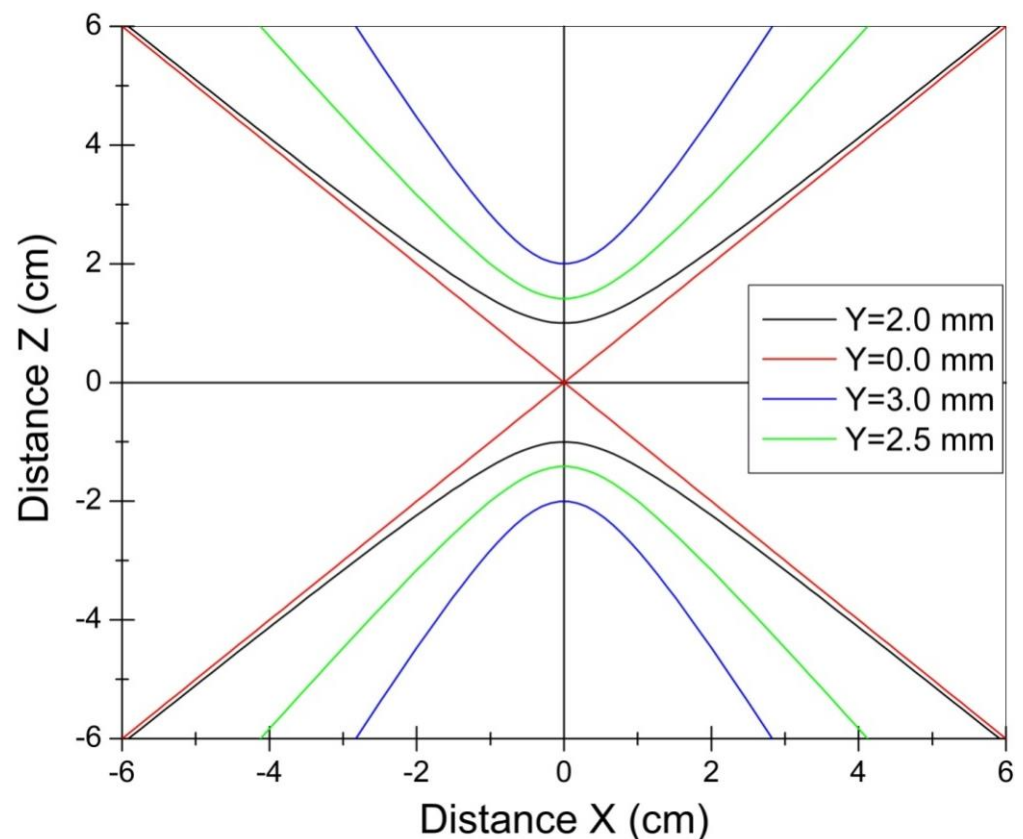


Figure 2. Hyperbolas representing the isogyres that are projected on the Ferroc cell as a function of the distance of the center of the magnetic dipole in relation to the y-axis. The horizontal and vertical lines that pass through the origin are also isogyres. The two red lines that pass through the diagonals are the limit for the formation of two hyperbolas.

The curved lines can be approximated by hyperbolas, and they represent the geometric locus where any of the components of the magnetic field B_x or B_z projected on the Ferroc cell cancels out, making this field aligned with the polarizer at the entrance of the light or with the analyzer.

Now that we have recognized some of the possible patterns in this system, we must consider the central question of this article, as follows: how do we explore these results in the context of the Mueller calculus?

One of the objectives of this work is to show how Mueller matrices can be used to analyze the light polarization properties observed in a thin film of ferrofluid, and the relevance of this work has two aspects. First, the answer to this question helps us understand some aspects of the magneto-optics of this system. Second, this experiment is an excellent tool for teaching light polarization caused by particle scattering. To develop this work relating the Mueller matrices with the luminous patterns of light polarization in a Ferroc cell, we will present our materials and methods in the next section, and then we will draw a parallel between the angular distribution of intensities and the types of polarization in an image obtained experimentally and with a Mueller matrix representing a radial grid. In the concluding section, we will make our final remarks.

2. Material and Methods

The ferrofluid used in the experiment is the EFH1 (Ferrotec) variety, with a saturation magnetization of 440 G, and 10 nm size single-domain iron oxide nanoparticles. The ferrofluid solution is placed between two glass plates, with each glass plate having a thickness variation of around 1 μm . The thin film has a thickness of around 10 μm . The response time for the ferrofluid is of the order of 200 ms, and the scattering pattern disappears almost instantly after removing the magnetic field. The ferrofluid is isotropic for very low magnetic fields. The source of the magnetic field is made using neodymium super magnets, which are placed close to the Ferroc cell, and the maximum magnetic field of the magnets used in this experiment is in the order of 1000 G. We have placed a video about the materials used in this video in the Supplementary Materials section to detail other aspects of this experiment.

In the present paper we are exploring the use of the Stokes vector, because Mueller matrices operate on such vectors and involve real parameters that can be measured directly with suitable optical instruments. The incident light is represented with a Stokes vector and the result obtained with the Ferroc cell acting on this incident light is the signal represented by another final Stokes vector. The Stokes parameters I , Q , U , and V are defined as the elements of a 4×1 column vector S of the components of the electric oscillations of light, which describes a full state of polarization with the couplet (θ, ϕ) as the polar angle and the azimuth angle, respectively. They are related with the Stokes vector S_{PP} observed in the patterns in a Ferroc cell with the six values of intensities, namely I_p , I_s , I_{+45} , I_{-45} , I_R , and I_L , as follows [2]:

$$S = \begin{bmatrix} I \\ Q \\ U \\ V \end{bmatrix} = \sqrt{\frac{\varepsilon}{\mu}} \begin{bmatrix} E_{0\theta}E_{0\theta}^* + E_{0\phi}E_{0\phi}^* \\ E_{0\theta}E_{0\theta}^* - E_{0\phi}E_{0\phi}^* \\ -2\text{Re}E_{0\theta}E_{0\phi}^* \\ 2\text{Im}E_{0\theta}E_{0\phi}^* \end{bmatrix} \Rightarrow S_{PP} = \begin{bmatrix} I_p + I_s \\ I_p - I_s \\ I_{+45} - I_{-45} \\ I_R - I_L \end{bmatrix} \quad (6)$$

With the final vector shown in Equation (6), we can find all the representation necessary to describe the polarization state of light that will be observed in this system.

An interesting graphic way to interpret the Stokes vector is to consider the approximation that this vector can be related to the S_i elements of the Poincaré sphere for the case of a completely polarized light beam. In this graphical representation, the radius of this sphere is S_0 , which represents the incident irradiance of the light beam, while S_x is the difference in radiant energy flux per unit area, or irradiances, between the horizontal I_p and vertical polarization I_s components of the beam. The preference for $+45^\circ$ or -45° polarization is given by S_y , and S_z is related to the influence of right or left circular polarization states that affect light.

In this way, any polarization state is defined by the vector oriented from the origin at the center of the sphere to a point on the surface of this sphere according to the following equation:

$$S_0^2 \geq S_x^2 + S_y^2 + S_z^2. \quad (7)$$

When the beam is fully polarized we have the identity and, when the beam is partially polarized, the square of S_0 is greater than the sum of the square of the components S_x , S_y , and S_z .

Now let us relate how the light at each point of the polarization pattern is related to its respective Stokes vector for the case of a dipole magnetic field applied to the plane where the thin film of ferrofluid is located in Figure 3. As discussed in our previous works [1,14], ferrofluid particles are oriented by the applied magnetic field, as if forming the field lines of Figure 3a. For the case of a system with a linear polarizer and linear analyzer, we have determined that the orientation of the polarization is perpendicular to these field lines. In this way, light polarization vectors parallel or perpendicular to one of the input or output elements of the polarizer/analyzer system will be blocked and, consequently, we will have dark regions in the polarization pattern, as is shown in Figure 3b. Points where the polarization of the light is at 45° in relation to any of the elements of the polarizing/analyzer system will have maximum light intensity. For the intermediate angles between these two cases, we will have the light intensity varying according to the projection on a trigonometric circle that is characteristic of harmonic functions.

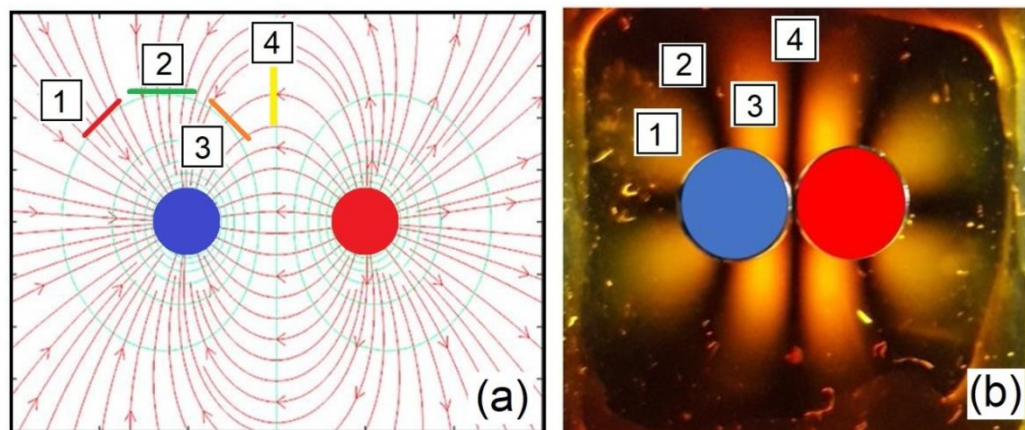


Figure 3. Diagram of the field lines of a magnetic dipole with linear polarization orientation at some points in (a), showing that the polarization of light is perpendicular to the field lines. (b) Image of the light pattern of a magnetic dipole for the ferrofluid sample placed between two crossed linear polarizers. In the figures, each number represents a type of linear polarization of light, as follows: (1) 45 degrees positive polarization (red), (2) horizontal polarization (green), (3) negative 45 degrees polarization (orange), (4) vertical polarization (yellow).

To verify if the light is partially polarized, we set up three different systems with this dipolar configuration. The first used a linear polarizer and a linear analyzer, and we obtained the image in Figure 4a. The second system used a linear polarizer, the Ferrocell, and a circular analyzer oriented to the right, and we obtained the following image in Figure 4b. Then, we changed the analyzer to another left-oriented circular polarizer and obtained the other image in Figure 4c.

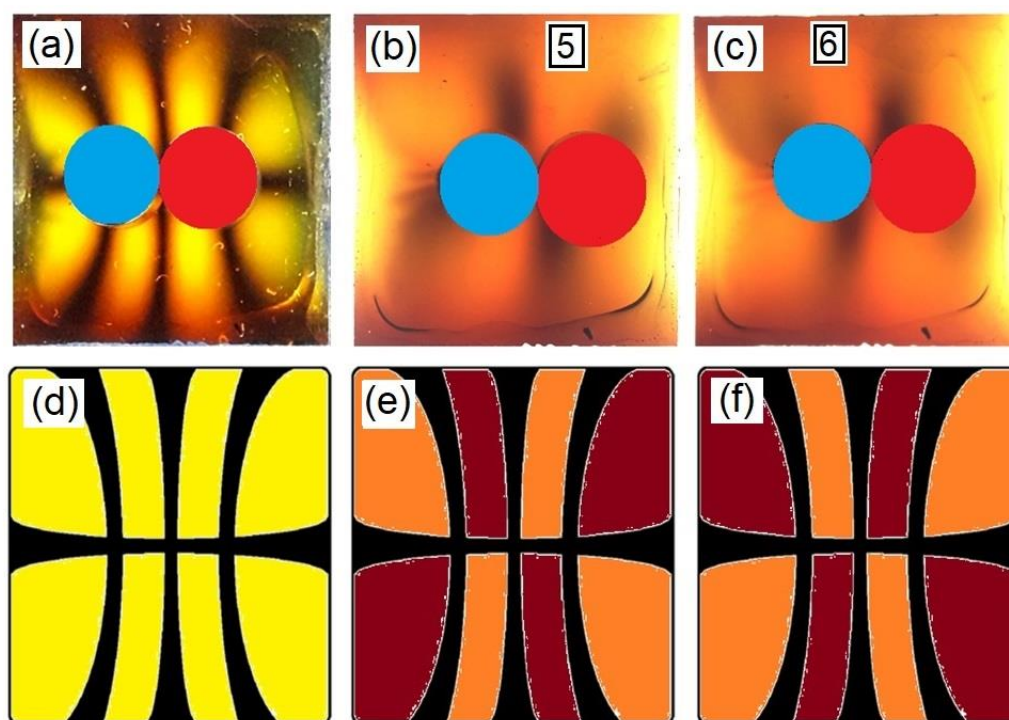


Figure 4. (a) Image of the linear polarization of a magnetic dipole. (b) Image of the polarization pattern of light with the same dipole, but with a linearly polarized light input and analyzed with a right-hand circular polarizer. (c) Image of the polarization pattern of light with the same dipole, but with a linearly polarized incoming light and analyzed with a left circular polarizer. In order to emphasize the polarization pattern, we have diagram (d) for the case shown in (a), the diagram in (e) for the case (b) and the diagram in (f) for the case in (c). Circular polarization patterns are complementary. With this experiment, we realized that the light that passes through the ferrofluid layer is partially polarized.

To emphasize the main differences between the three patterns, we made diagrams of Figure 4d–f. The first point we notice is the intensities of the light patterns for the case involving circular analyzers. Another interesting aspect is that we have an alternation in the most intense regions with circular polarization when compared to the case of linear polarization shown in Figure 4d; in addition, the light patterns obtained with the analyzers with circular polarization are complementary, as we can see in the diagrams of Figure 4e,f. With these observations, we can conclude that linearly polarized light becomes partially polarized when passing through ferrofluid, with linear and circular components, depending on the orientation of the magnetic field.

Considering the ideal cases of light polarization shown in the previous light patterns with the numbers 1, 2, 3, 4 for linear polarization and 5 and 6 for circular polarization, we present Figure 5 with the Stokes vectors for the ideal cases of polarization. In order to find the partial polarization cases in our system with ferrofluids, we will now analyze some Mueller matrices operating on some input Stokes vectors.

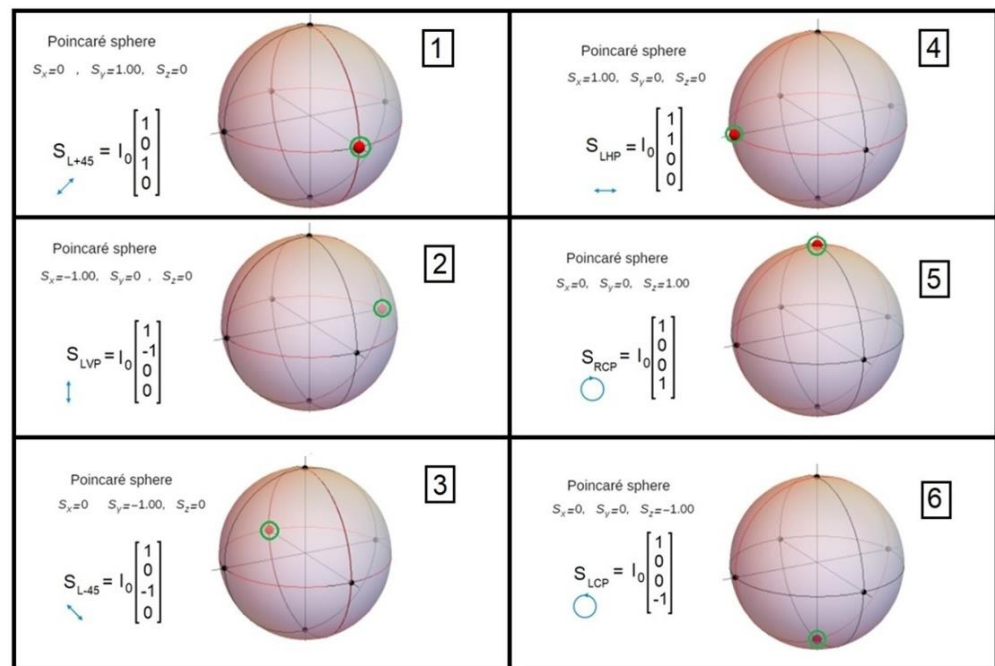


Figure 5. Stokes vectors and Poincaré sphere for the light polarization observed in the pattern of a dipolar magnetic field for a Ferrocene. Each number represents a type of light polarization, as follows: (1) 45 degrees positive polarization, (2) horizontal polarization, (3) negative 45 degrees polarization, (4) vertical polarization, (5) right-hand circular polarization, and (6) left-hand circular polarization.

3. Mueller Matrices and Light Patterns

The Mueller matrix describes the Stokes vector after the interaction with matter, and the interaction between light and the sample for the case of the Mueller matrix and Stokes vector is represented by the linear transformation of an incident Stokes vector S_0 to an outgoing Stokes vector S_1 due to the 4×4 Mueller matrix M , as follows:

$$S_1 = M \cdot S_0 \Rightarrow S_1 = \begin{bmatrix} m_{11} & m_{12} & m_{13} & m_{14} \\ m_{21} & m_{22} & m_{23} & m_{24} \\ m_{31} & m_{32} & m_{33} & m_{34} \\ m_{41} & m_{42} & m_{43} & m_{44} \end{bmatrix} S_0. \tag{8}$$

In order to study the effects of the polarization of light in a thin film of ferrofluid for a radial field manipulating Stokes vectors, we use a matrix that simulates a radial polarizer [17] for the case of radially symmetrical magnetic fields for the angle θ and the parameter q , such as in the following case of a monopolar magnetic field:

$$M_1 = \frac{1}{2} \begin{bmatrix} 1 & \cos(2q\theta) & \sin(2q\theta) & 0 \\ \cos(2q\theta) & \cos(2q\theta)^2 & \sin(2q\theta) \cos(2q\theta) & 0 \\ \sin(2q\theta) & \sin(2q\theta) \cos(2q\theta) & \sin(2q\theta)^2 & 0 \\ 0 & 0 & 0 & 0 \end{bmatrix} \tag{9}$$

We start by simulating the case where the light incident on the Ferrocene is left circularly polarized, represented by the Stokes *CircL* vector, and the analyzer is a right homogeneous circular polarizer A_2 , for the case of a symmetrical magnetic field centered at the magnet, as follows:

$$CircL = \begin{bmatrix} 1 \\ 0 \\ 0 \\ -1 \end{bmatrix}, A_2 = \frac{1}{2} \begin{bmatrix} 1 & 0 & 0 & 1 \\ 0 & 0 & 0 & 0 \\ 0 & 0 & 0 & 0 \\ 1 & 0 & 0 & 1 \end{bmatrix}. \tag{10}$$

The corresponding output Stokes vector has a right circular polarization that is attenuated to a quarter of the initial value, represented in the polar plot of Figure 6a, considering an angular variation with a fixed radius. This can be verified by the experiment, with a region of white-colored maximum intensity around the magnet shown in Figure 6b.

$$S_1 = A_2 \cdot M_1 \cdot \text{CircL} \Rightarrow S_1 = \begin{bmatrix} \frac{1}{4} \\ 0 \\ 0 \\ \frac{1}{4} \end{bmatrix}. \quad (11)$$

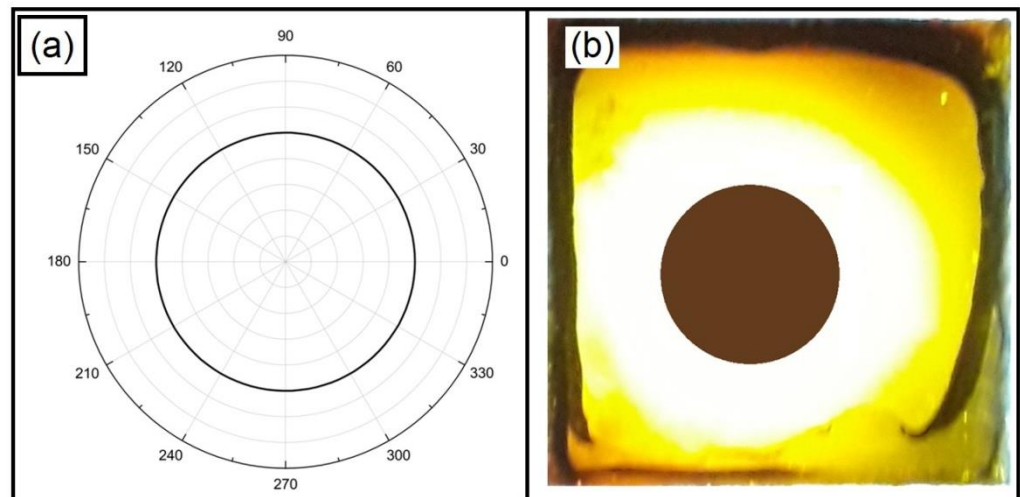


Figure 6. Polar plot for the Stokes vector intensity parameter S_1 in (a) of Equation (11). (b) Polarization image obtained with a Ferrocell for an incoming light circularly polarized to the left and analyzed with a circular polarizer to the right.

It is interesting to note that circularly polarized light switches from left polarization to right polarization after passing through the Ferrocell, as in the case of polarization inversion for the reflection of waves of circularly polarized light.

The effects of polarization depend on the strength of the field, and we can have the same polarization of light in the region defined by this circumference for a monopolar field with the magnet at the center of the cell, or for a field that is formed by a magnetic ring with poles located on each side face of the ring. The difference between each case will be restricted to the intensity in the radial direction.

In this way, circular polarization can also be seen in the case of a magnet in the form of an axially magnetized ring, as shown in Figure 7, which occurs mainly in the region close to the ring, where we have the maximum field strength.

Now let us apply this Mueller matrix to the case of incidence of a linearly polarized light represented by the Stokes vector $VerP$ and with a linear analyzer represented by a matrix A_1 , as follows:

$$VerP = \begin{bmatrix} 1 \\ -1 \\ 0 \\ 0 \end{bmatrix}, \quad A_1 = \frac{1}{2} \begin{bmatrix} 1 & 1 & 0 & 0 \\ 1 & 1 & 0 & 0 \\ 0 & 0 & 0 & 0 \\ 0 & 0 & 0 & 0 \end{bmatrix}. \quad (12)$$

For the case of the matrix M_1 we have the following Stokes vector as an answer:

$$S_1 = A_1 \cdot M_1 \cdot VerP \Rightarrow S_1 = \begin{bmatrix} \frac{1}{4} - \frac{1}{4}(\cos(\theta))^2 \\ \frac{1}{4}(\cos(\theta))^2 - \frac{1}{4} \\ 0 \\ 0 \end{bmatrix}. \quad (13)$$

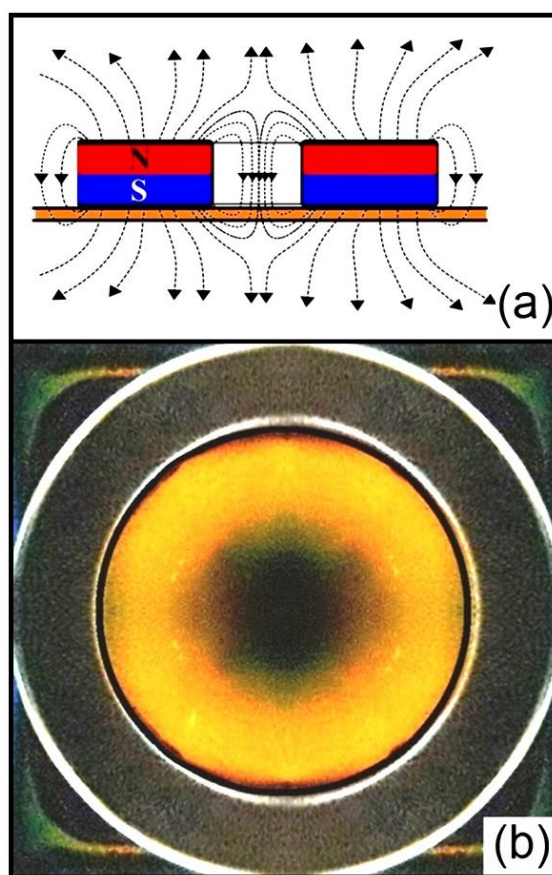


Figure 7. Diagram of the magnetic ring with field lines on the Ferrocell (a). Image of the experiment in (b) taking as its input the light circularly polarized to the left and analyzed with a polarizer to the right.

The parameter I of the Stokes vector S_1 can be compared with the experimental result obtained in our experiment, as shown in the Figure 8, in which the ferrofluid sample is in the presence of a magnet with one of the poles at the center of the Ferrocell, known as a monopolar configuration. The ferrofluid is between two crossed linear polarizers. The light pattern obtained in Figure 8a is in the form of four luminous lobes separated by two crossed isogyres. The region marked by the green circles is the region where the light intensity is measured for all angles. In Figure 8b, there is a graph in polar coordinates comparing experimental data of light intensity (points) with Malus' law represented by the red line. This case is similar to the case of polarization of light which gives us Malus' law for an angular variation within a closed circle [16].

We have already seen that in the case of a magnetic dipole with two crossed linear polarizers, we have a pattern of light polarization with eight luminous lobes with radial symmetry and formation of hyperbolic isogyres. The limiting case would occur when the hyperbolas become lines. In practice this would correspond to the center of the magnetic dipole crossing the thin film layer of ferrofluid. This is difficult to do because of fluid leakage. However, we can obtain an equivalent configuration using the magnetic field of one sextupole of Figure 9. A sextupole magnetic field consists of six magnetic poles (Figure 9a) placed in an alternating arrangement of north and south poles arranged around an axis. We used this arrangement to obtain the luminous pattern that is shown in Figure 9b, in which we have vertically polarized light passing through the ferrofluid, which was then analyzed with a horizontal linear polarizer.

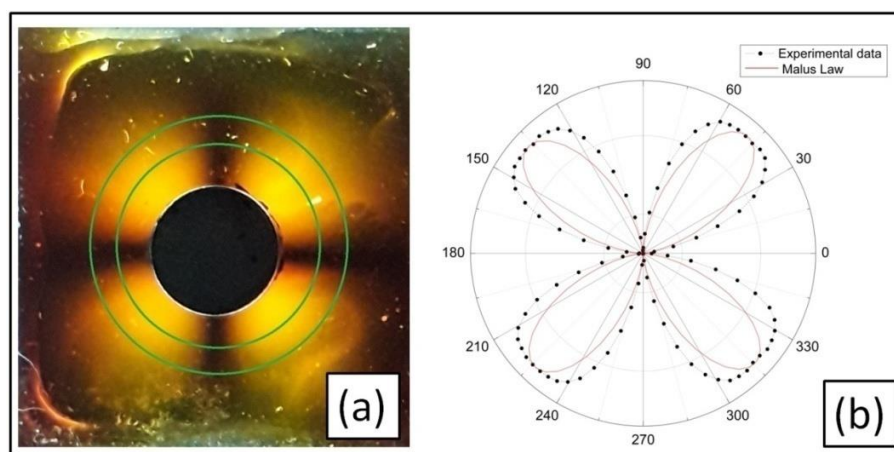


Figure 8. Checking Malus’ law using a Ferrocell. The ferrofluid sample is in the presence of a magnet with one of the poles at the center of the Ferrocell, known as a monopolar configuration. The ferrofluid is between two crossed linear polarizers. The light pattern obtained in (a) is in the form of four luminous lobes separated by two crossed isogyres. The region marked by the green circles is the region where the light intensity is measured for all angles. (b) Graph in polar coordinates comparing experimental data of light intensity (points) with Malus’ law represented by the red line.

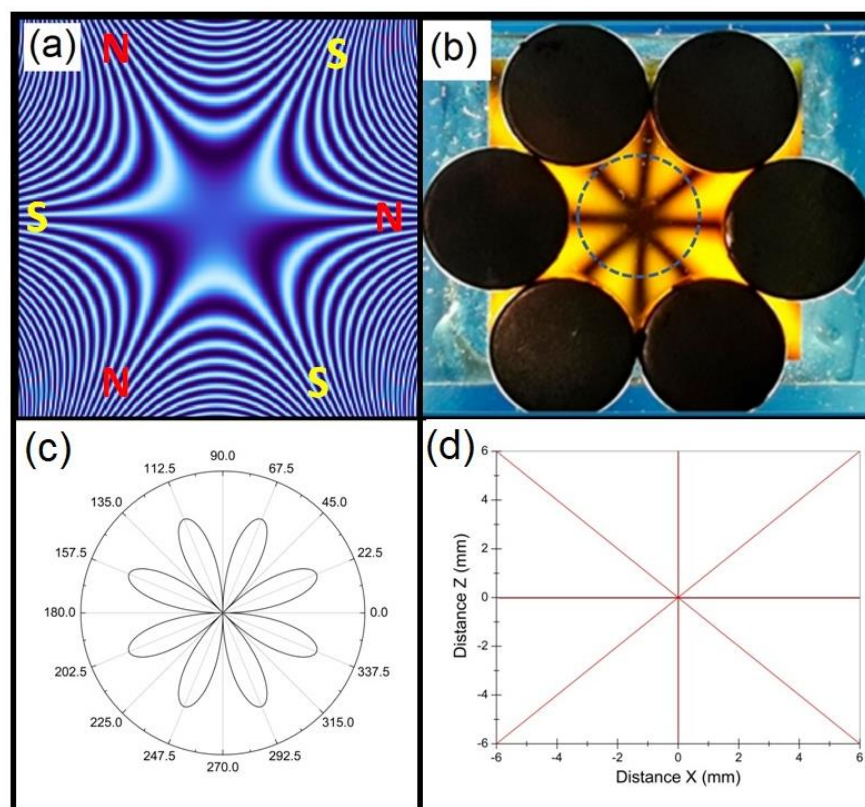


Figure 9. (a) Line intensity diagram of a sextupolar magnetic field. (b) Six magnetic disks forming a sextupolar field in the ferrofluid sample for a pair of crossed linear polarizers. (c) Polar graph of the intensity of the Stokes vector S for the Mueller matrix, simulating a grating of a sextupolar magnetic field, which is equivalent to what was observed for the light intensity in the experiment, as marked with the circle with the green dashed line in (b). In (d), there is the graph of the isogyres lines of a sextupole, which uses Equations (2) and (3) to explain the isogyres for a dipole for $y = 0.0$ mm.

Now, due to the symmetry of the magnetic field, we have considered the parameter $q = 2$ for the Mueller matrix M_1 , and we have obtained the following Stokes vector $S_{\text{sextupole}}$:

$$M_1 = \frac{1}{2} \begin{bmatrix} 1 & \cos(4\theta) & \sin(4\theta) & 0 \\ \cos(4\theta) & \cos(4\theta)^2 & \sin(4\theta)\cos(4\theta) & 0 \\ \sin(4\theta) & \sin(2q\theta)\cos(4\theta) & \sin(4\theta)^2 & 0 \\ 0 & 0 & 0 & 0 \end{bmatrix}, \quad (14)$$

$$S_{\text{sextupole}} = A_1 \cdot M_1 \cdot \text{VerP} \Rightarrow S_1 = \begin{bmatrix} \frac{1}{4} - \frac{1}{4}(\cos(4\theta))^2 \\ \frac{1}{4} - \frac{1}{4}(\cos(4\theta))^2 \\ 0 \\ 0 \end{bmatrix}. \quad (15)$$

The result obtained with the Stokes $S_{\text{sextupole}}$ vector confirms the formation of the eight luminous lobes of Figure 9c for the parameter I of Equation (15), and the limiting case of straight isogyres of Figure 9d, already discussed for the dipole case.

In Figure 10, we present a direct comparison between the results obtained with the experiment for the case where we applied a sextupolar field in the Ferrocell and the simulation for this same case obtained with the intensity parameter I of the Stokes vector of Equation (15).

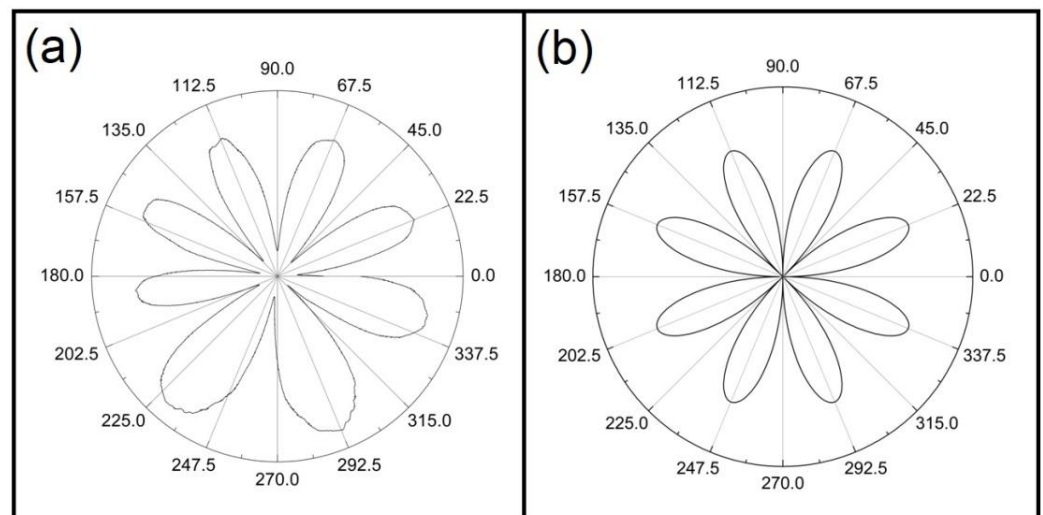


Figure 10. Intensity plots for linear polarization when applying a sextupolar magnetic field to the ferrofluid. In (a) we have the graph obtained from the experiment with the luminous pattern of Figure 9b in the region demarcated with the circumference made with the green dashed line. In (b) we have the intensity graph obtained with the Stokes vector of Equation (15).

Although the Mueller matrix reasonably represents the in-plane angular distribution of the Ferrocell thin film, it does not account for cell thickness. This can be observed for the case of light polarization in the case of the magnetic dipole, or in the case of the sextupolar magnet, when the ferrofluid interacts with circularly polarized light, as shown in Figure 11. In Figure 11a, we see the light pattern of polarization, in which a linearly polarized light is injected into the ferrofluid, leaving it partially circularly polarized. In the patterns of Figure 11, just as in Figure 4, we see by contrast that the light is blocked in some parts and not in others. The same happens with the light pattern shown in Figure 11b. The respective intensity parameters of these Stokes vectors are shown in Figure 11c,d. We can see from the experiment that the patterns are approximately complementary, as we have already mentioned for the case of the luminous pattern obtained with the magnetic dipole in Figure 4, in such a way that the polarization “petals” of Figure 10 alternate, with four maximum intensities, as shown in the polar graphs of Figure 11c,d.

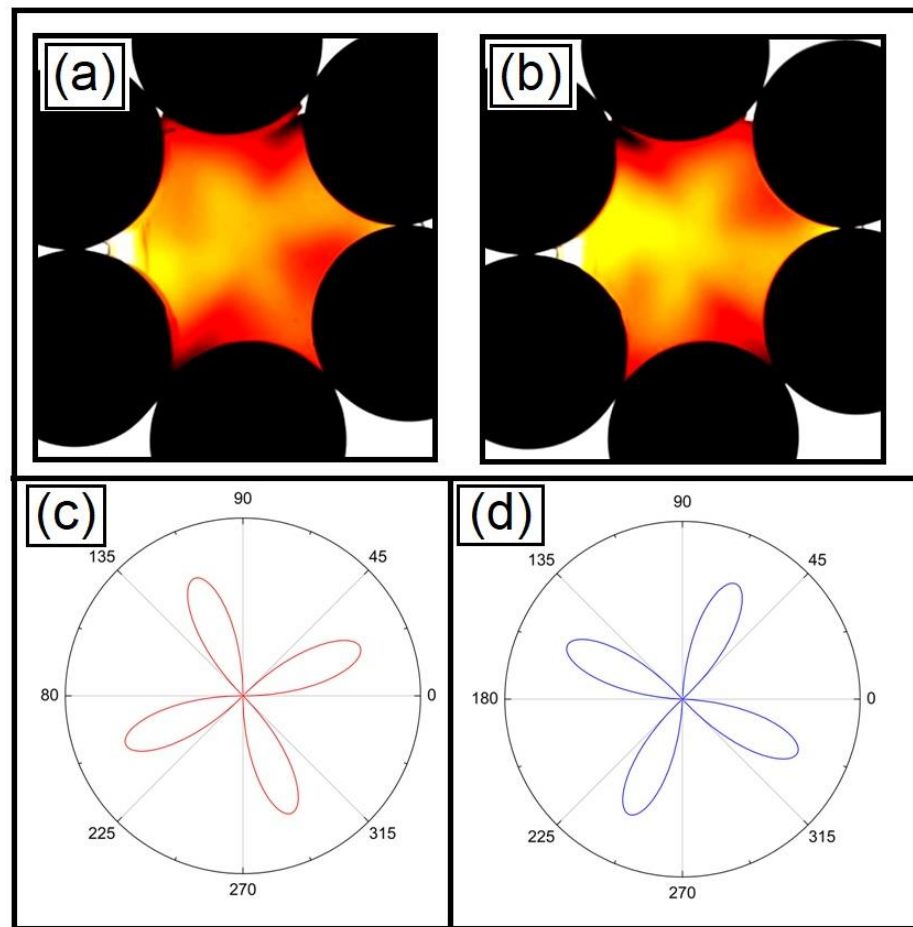


Figure 11. Circular polarization in Ferrocell for a sextupolar magnetic field. The light entering the Ferrocell is linearly polarized light. In (a) we have the light that emerges from the Ferrocell being analyzed with a circular polarizer to the right, and in (b) the light is analyzed with a circular polarizer oriented to the left. In (c) we have the graph in polar coordinates of the light intensity for the case of the image in (a), while in (d) we have the graph in polar coordinates for the intensity of light for the case in (b).

Following the experimental results, the Stokes vectors representing the polarization plots of Figure 11c for right circular polarization S_{red} , and Figure 11d for left circular polarization S_{blue} could be represented by the following Equation (16):

$$S_{red} = a \begin{bmatrix} 1 - \{2 \cos[2(\theta + 22.5)]\}^2 \\ Q \\ U \\ 1 \end{bmatrix}, \quad S_{blue} = a \begin{bmatrix} 1 - \{2 \cos[2(\theta - 22.5)]\}^2 \\ Q \\ U \\ -1 \end{bmatrix}. \quad (16)$$

This may be related to the fact that the dichroism is linked to the diffraction grating pattern with spatial orientation in a plane, while the Ferrocell thickness is linked to the elastic scattering of light, which gives rise to polarization states different from those of the incident beam. Thus, for a thickness in the order of tens of 10 μm , the ferrofluid particles extract a part of the incident energy and scatter it in all directions, at the same frequency as the incident beam, as if it were some kind of birefringence. For future work, we suggest the analysis of the use of Mueller matrices that represent quarter-wave plates that consist of a spatially variable retarder with phase shift and optical axis orientation.

Graphs in polar coordinates of left and right circular light polarization are shown in Figure 12a,b, for three different data sets of patterns similar to the case observed in

Figure 11a,b. These curves are further from the origin than in the case of linear polarization, as shown in Figure 12c, which indicates a lower contrast between the light and dark regions in the polarization patterns. As there is a coexistence of different types of light polarization, we note that, for the case of linear polarization, we have greater amplitude between the maximum and minimum values of intensity when compared to the case of linear polarization, as can be seen in Figure 12.

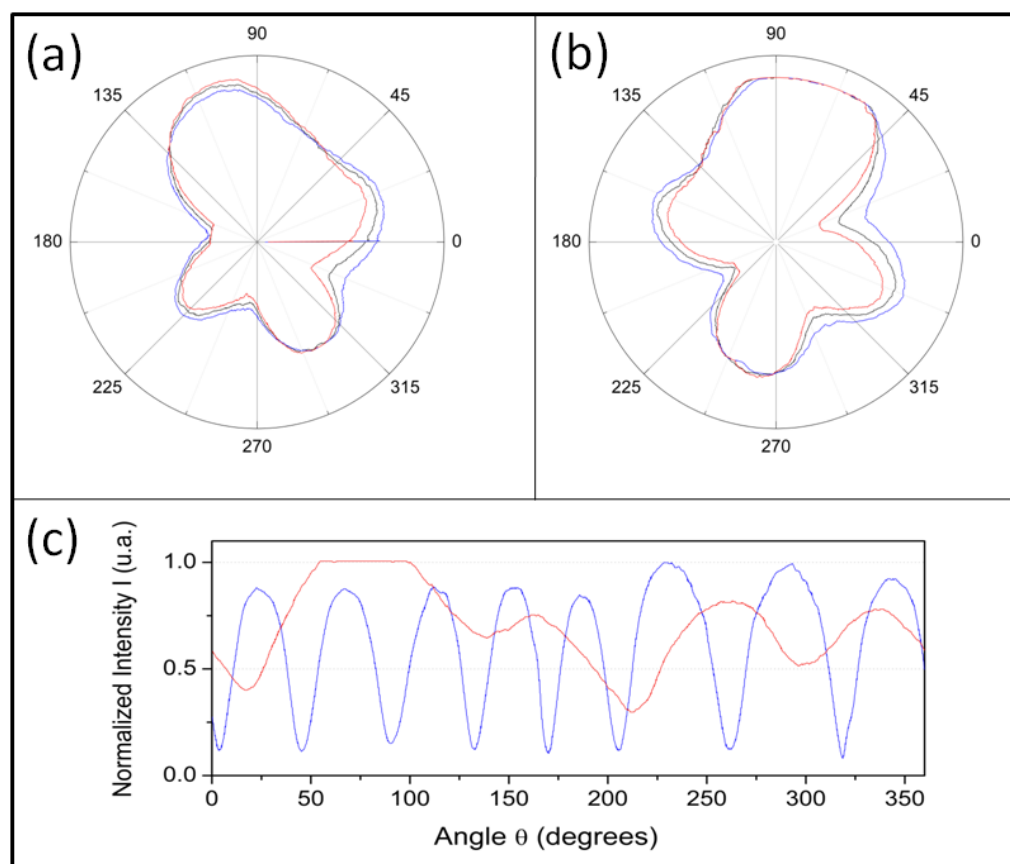


Figure 12. Graphs in polar coordinates of the circular polarization of light to the right (a) and to the left (b), for three data sets each represented with the color red, black, and blue. (c) Comparison between the polarization of light between the linear case represented with the curve in blue and the case of circular polarization represented in red.

4. Conclusions

We have studied the polarization of light in a thin film of ferrofluid subjected to a magnetic field using the formalism of the Mueller matrix. As far as we know, for the first time, we presented through experiments how to relate light patterns with Stokes vectors and how they can be operated by Mueller matrices related to the magnetic field applied to the ferrofluid. We have observed that the changes in the dichroism of this system can be monitored throughout the sample, allowing the visualization of magneto-optical effects mainly for linear polarized light, and the effects of circular polarized light are related to birefringence.

In our modeling process, we see that a crucial point is the description of the magnetic field in an angular coordinate system that can be represented in a matrix form, because the nanoparticles will align with the magnetic field.

Compared with experimental systems where the Mueller calculation is usually applied, our experiment allows a direct visualization of the polarization phenomena, in addition to a flexibilization of the patterns generated due to the formation of diffraction gratings for different magnetic field configurations. Furthermore, we observed in this work that

different types of light polarization can coexist, indicating that the ferrofluid film forms a more complex structure than a simple diffraction grating when a magnetic field is applied.

Supplementary Materials: The following supporting information can be downloaded at: <https://iframe.videodelivery.net/6ce692827f8149c2948bd30531ccea1b> “Light Polarization by Ferrofluid Film Using Jones Calculus”.

Author Contributions: Conceptualization, A.T. and A.P.B.T.; methodology, A.T.; software, A.T.; validation, A.T. and A.P.B.T.; formal analysis, A.T.; investigation, A.T.; resources, A.T.; data curation, A.T.; writing—original draft preparation, A.T.; writing—review and editing, A.T.; visualization, A.T.; supervision, A.T.; project administration, A.T.; funding acquisition, A.T. and A.P.B.T. All authors have read and agreed to the published version of the manuscript.

Funding: This work was partially supported by Conselho Nacional de Desenvolvimento Científico e Tecnológico (CNPq), Instituto Nacional de Ciência e Tecnologia de Fluidos Complexos (INCT-FCx), and by Fundação de Amparo à Pesquisa do Estado de São Paulo (FAPESP) FAPESP/CNPq#573560/2008-0.

Acknowledgments: A.T. and A.P.B.T. thank Conselho Nacional de Desenvolvimento Científico e Tecnológico (CNPq), Instituto Nacional de Ciência e Tecnologia de Fluidos Complexos (INCT-FCx), and Fundação de Amparo à Pesquisa do Estado de São Paulo (FAPESP).

Conflicts of Interest: The authors declare no conflict of interest.

References

1. Tufaile, A.; Vanderelli, T.A.; Tufaile, A.P.B. Light polarization using ferrofluids and magnetic fields. *J. Adv. Condens. Matter Phys.* **2017**, *2017*, 2583717. [[CrossRef](#)]
2. Mischchenko, M.I.; Travis, L.D.; Laci, A.A. *Scattering, Absorption, and Emission of Light by Small Particles*; Cambridge University Press: Cambridge, UK, 2002.
3. Hecht, E. *Optics*; Addison-Wesley Longman: Boston, MA, USA, 1998; Available online: <https://www.amazon.com/Optics-4th-Eugene-Hecht/dp/0805385665> (accessed on 6 October 2022).
4. Manjunatha, B.S.; Agrawal, A.; Shah, V. Histopathological evaluation of collagen fibers using picosirius red stain and polarizing microscopy in oral squamous cell carcinoma. *J. Cancer Res. Ther.* **2015**, *11*, 272. [[CrossRef](#)] [[PubMed](#)]
5. He, C.; He, H.; Chang, J.; Dong, Y.; Liu, S.; Zeng, N.; He, Y.; Ma, H. Characterizing microstructures of cancerous tissues using multispectral transformed mueller matrix polarization parameters. *Biomed. Opt. Express* **2015**, *6*, 2934–2945. [[CrossRef](#)] [[PubMed](#)]
6. Zhang, Y.; Lee, S.Y.C.; Zhang, Y.; Furst, D.; Fitzgerald, J.; Ozcan, A. Wide-field imaging of birefringent synovial fluid crystals using lens-free polarized microscopy for gout diagnosis. *Sci. Rep.* **2016**, *6*, 1–14. [[CrossRef](#)] [[PubMed](#)]
7. Lizana, A.; Foldyna, M.; Stchakovsky, M.; Georges, B.; Nicolas, D.; Garcia-Caurel, E. Enhanced sensitivity to dielectric function and thickness of absorbing thin films by combining total internal reflection ellipsometry with standard ellipsometry and reflectometry. *J. Phys. D Appl. Phys.* **2013**, *46*, 105501. [[CrossRef](#)]
8. Mendoza-Galván, A.; Muñoz-Pineda, E.; Ribeiro, S.J.; Santos, M.V.; Järrendahl, K.; Arwin, H. Mueller matrix spectroscopic ellipsometry study of chiral nanocrystalline cellulose films. *J. Opt.* **2018**, *20*, 024001. [[CrossRef](#)]
9. López-Morales, G.; Sánchez-López, M.M.; Lizana, A.; Moreno, I.; Campos, J. Mueller Matrix Polarimetric Imaging Analysis of Optical Components for the Generation of Cylindrical Vector Beams. *Crystals* **2020**, *10*, 1155. [[CrossRef](#)]
10. Hough, J. Polarimetry: A powerful diagnostic tool in astronomy. *Astron. Geophys.* **2006**, *47*, 31–35. [[CrossRef](#)]
11. Tyo, J.S.; Goldstein, D.L.; Chenault, D.B.; Shaw, J.A. Review of passive imaging polarimetry for remote sensing applications. *Appl. Opt.* **2006**, *45*, 5453–5469. [[CrossRef](#)] [[PubMed](#)]
12. Arteaga Barriel, O. Mueller Matrix Polarimetry of Anisotropic Chiral Media. Ph.D. Thesis, Universitat de Barcelona, Barcelona, Spain, 2010.
13. Misson, G.P.; Temple, E.; Anderson, J. Computational simulation of Haidinger’s brushes. *J. Opt. Soc. Am. A Opt. Image* **2018**, *35*, 946–952. [[CrossRef](#)] [[PubMed](#)]
14. Tufaile, A.; Snyder, M.; Tufaile, A.P.B. Horocycles of Light in a Ferrocylinder. *Condens. Matter.* **2021**, *6*, 30. [[CrossRef](#)]
15. Snik, F.; Craven-Jones, J.; Escuti, M.; Fineschi, S.; Harrington, D.; de Martino, A.; Mawet, D.; Riedi, J.; Tyo, J.S. An overview of polarimetric sensing techniques and technology with applications to different research fields. *Polariz. Meas. Anal. Remote Sens.* **2014**, 9099, 90990B. [[CrossRef](#)]
16. Tufaile, A.; Snyder, M.; Tufaile, A.P.B. Study of Light Polarization by Ferrofluid film using Jones Calculus. *Condens. Matter.* **2022**, *7*, 28. [[CrossRef](#)]
17. Jourlin, Y.; Tonchev, S.; Parriaux, O.; Zeitner, U. Waveguide Grating Radial Polarizer for the Photolithography of Circularly Symmetrical Optical Elements. *IEEE Photonics J.* **2012**, *4*, 1728–1736. [[CrossRef](#)]